Comparisons of snowmelt detected by microwave sensors on the Shackleton Ice Shelf, East Antarctica

Article *in* International Journal of Remote Sensing · September 2019

DOI: 10.1080/01431161.2019.1666316

2 authors:

Lei Zheng
Sun Yat-Sen University
23 PUBLICATIONS **203** CITATIONS
SEE PROFILE

Chunxia Zhou
Wuhan University
41 PUBLICATIONS **288** CITATIONS
SEE PROFILE

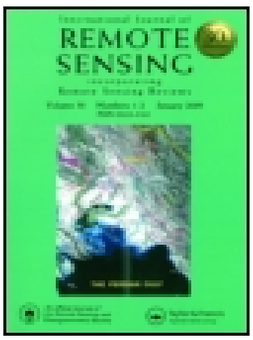

International Journal of Remote Sensing

ISSN: 0143-1161 (Print) 1366-5901 (Online) Journal homepage: https://www.tandfonline.com/loi/tres20

Comparisons of snowmelt detected by microwave sensors on the Shackleton Ice Shelf, East Antarctica

Lei Zheng & Chunxia Zhou

To cite this article: Lei Zheng & Chunxia Zhou (2019): Comparisons of snowmelt detected by microwave sensors on the Shackleton Ice Shelf, East Antarctica, International Journal of Remote Sensing, DOI: 10.1080/01431161.2019.1666316

To link to this article: https://doi.org/10.1080/01431161.2019.1666316

Published online: 16 Sep 2019.

INTERNATIONAL JOURNAL OF REMOTE SENSING
https://doi.org/10.1080/01431161.2019.1666316

Taylor & Francis
Taylor & Francis Group

Comparisons of snowmelt detected by microwave sensors on the Shackleton Ice Shelf, East Antarctica

Lei Zheng and Chunxia Zhou

Chinese Antarctic Center of Surveying and Mapping, Wuhan University, Wuhan, China

ABSTRACT

Surface snowmelt is of great importance to the ice sheet's mass and energy balance. Microwave sensors, including radiometer and scatterometer can be used to map snowmelt. Two new microwave sensors, including the Advanced Microwave Scanning Radiometer 2 (AMSR2) and the Advanced Scatterometer (ASCAT), were compared in terms of their behaviours in snowmelt detection on the Shackleton Ice Shelf (SIS) in East Antarctica. Melt signals were determined by identifying the sharp changes in AMSR2 brightness temperature and ASCAT backscatter. The results suggest that the SIS began to melt in December, melt area shrank quickly in February after reaching the peak in January. Melt area mapped by the two sensors agreed with each other on the SIS, however, also shows local discrepancies in the places with complex terrains. ASCAT failed to recognized melt signals in the regions with blue ice and rock outcrops where extensive melt ponds were observed based on Landsat 8 images. Snowmelt detected by radiometer and scatterometer shows complementary nature, the combination of multisource remote sensing images is expected to provide a better view of the ice sheet surface melting conditions.

ARTICLE HISTORY
Received 2 January 2019
Accepted 13 July 2019

1. Introduction

The emergence of liquid water in snowpack can greatly decrease the surface albedo and hence increase the snow temperature (Fraser et al. 2016). Heavy snowmelt may endanger the ice shelves when meltwater fills and enlarge the crevasses, and even lead to their break-ups (Scambos et al. 2000). So the monitoring of snowmelt is of great importance in the study of the stability, mass and energy balance of polar ice sheets. In situ measurements of snowmelt in the polar regions are limited because of the remoteness and abominable weather conditions. Spaceborne microwave sensors can be used to monitor freeze thaw cycles over the ice sheets due to their insensitivity to atmospheric and illumination conditions (Ashcraft and Long 2006). Microwave emissivity and absorptivity increase significantly even when the liquid water is only one percent in volume (Hallikainen, Ulaby, and Abdelrazik 1986), leading to the sharp increases of brightness temperature (T_b) and decreases of backscattering coefficient (σ^o).

CONTACT Chunxia Zhou zhoucx@whu.edu.cn Chinese Antarctic Center of Surveying and Mapping, Wuhan University, Wuhan 430079, China

Radiometers and scatterometers have large spatial coverages and high temporal resolutions which are able to monitor the quick changes in surface snowmelt. With a long time series of T_b measurements, radiometers can be used to study the snowmelt dynamics based on the T_b temporal variations (Tedesco, Abdalati, and Zwally 2007; McCabe, Chylek, and Dubey 2011). Similar to the radiometers, scatterometers detect melt signals by recognizing the rapid changes in σ°. Thresholding methods determined snowmelt when T_b or σ° increases or decreases to a certain value (Zheng et al. 2018; Kuipers Munneke et al. 2018). Edge detection methods were also used to identify the transitions of freeze thaw cycles (Liu, Wang, and Jezek 2005; Steiner and Tedesco 2014).

The responses of T_b and σ° to melt signals were found to vary with different liquid water content and the depth of the melting layer. Previous studies have found differences in snowmelt derived by passive and active microwave sensors (Ashcraft and Long 2006; Liu, Wang, and Jezek 2006; Steiner and Tedesco 2014; Zheng, Zhou, and Liang 2019). To examine the reasons for the local discrepancies of melt signals derived from radiometer and scatterometer, the Advanced Microwave Scanning Radiometer 2 (AMSR2) and Advanced Scatterometer (ASCAT) were compared in terms of their behaviours in snowmelt detection on the Shackleton Ice Shelf (SIS), East Antarctica.

2. Study area and data set

2.1. Study area

The SIS covers 33,820 km^2 in East Antarctica, hugging the coast for 384 km from 90° E to 105° E (Figure 1). Northcliffe, Denman and Scott Glacier flow into the sea via the SIS, the speed of the ice flow can reach 1500 m year^{-1} (Zwally et al. 2002; Urbini et al. 2010). As the northernmost ice shelf in East Antarctica, SIS's proximity to the continental shelf allows the evaluation of its susceptibility in light of climate change (Urbini et al. 2010).

2.2. Data set

As a successor of the Advanced Microwave Scanning Radiometer – Earth Observing System (AMSR-E), AMSR2 onboard the Global Change Observation Mission – Water 'Shizuku'(GCOM-W1) satellite was launched on 18 May 2012. From about 700 km above the Earth, AMSR2 obtains data over a 1450 km swath (Hihara, Kubota, and Okuro 2015). AMSR2 observes the Antarctic in afternoon and midnight for the ascending and descending passes respectively. The instantaneous field of view dimensions is approximately 7 km × 12 km at 36.5 GHz. AMSR2 Ka band vertically polarized T_b used in this study were obtained from the Japan Aerospace Exploration Agency with a sampling Interval of 10 km (Imaoka et al. 2010).

From about 817 km above the Earth, C band (5.2 GHz) ASCAT obtains data over a 1450 km swath (Figa-Saldaña et al. 2002). The effective resolution of ASCAT backscatter measurements is 12 km – 15 km in most areas. To improve the utility of the data set, the 4.45 km Scatterometer Image Reconstruction (SIR) product have been developed by the National Aeronautics and Space Administration (NASA) Scatterometer Climate Record Pathfinder project (Long, Hardin, and Whiting 1993). The ASCAT SIR product was obtained from Brigham Young University (Lindsley and Long 2010). The 10 km AMSR2 T_b were reprojected and resampled to the same spatial resolution as the ASCAT (4.45 km).

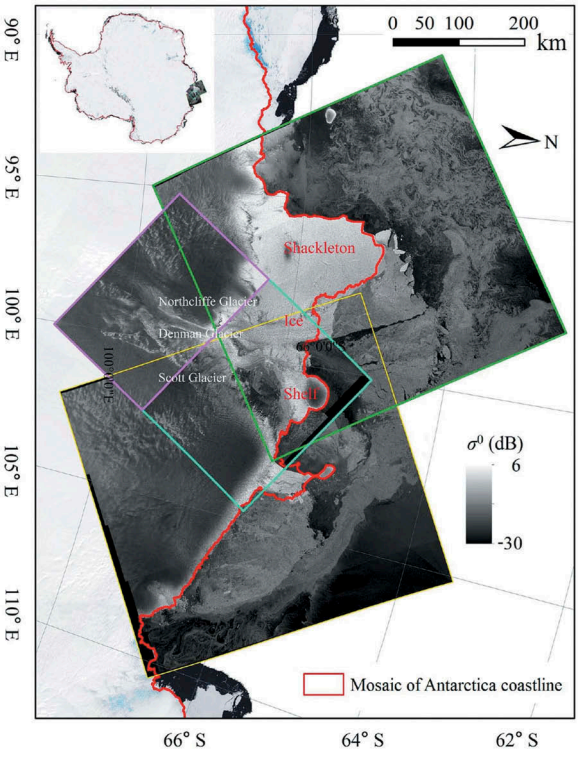

Figure 1. SIS and its location in the Antarctic. The Mosaic of Antarctica (MOA) coastlines (red line) were obtained from National Snow and Ice Data Centre (NSIDC) (Scambos et al. 2007). Base maps with coloured frames were the Sentinel 1 images from March to June in 2015 obtained from European Space Agency (ESA) (Torres et al. 2012).

3. Methodology

3.1. AMSR2 and ASCAT snowmelt detection

Snowmelt causes shifts to high diurnal amplitude variations in 36.5 GHz vertically polarized T_b (DAV_V^{36}) (Apgar et al. 2007), especially for the transitions in freeze thaw cycles (Zheng et al. 2018):

$$DAV_V^{36} = T_{b,VA}^{36} - T_{b,VD}^{36} \tag{1}$$

where $T_{b,VA}^{36}$ and $T_{b,VD}^{36}$stand for vertically polarized 36.5 GHz T_b in ascending and descending passes respectively. Melt signals have been successfully detected when the difference between the two passes exceeds 18 K (Monahan and Ramage 2010; Semmens et al. 2013). Similarly, Tedesco (2007) determined melt signals on the Greenland Ice Sheet when the vertically polarized 37.0 GHz diurnal amplitude T_b variations of the Special Sensor Microwave Imager (SSM/I) exceeds 18 K. We set the same threshold to detect snowmelt on the SIS based on DAV_V^{36}:

$$m(t) = \begin{cases} 1, DAV_V^{36}(t) & \geq 18K \\ 0, DAV_V^{36}(t) & < 18K \end{cases} \tag{2}$$

where t is time, $m(t)$ represents the daily freeze/thaw state with $m = 1$ indicating melting and $m = 0$ indicating frozen.

Liquid water leads to significant decreases of σ° compared with the winter observations. For C band backscattering measurements, melt signals are determined when σ° is at least 3 dB lower than the winter measurements (Luckman et al. 2014):

$$m(t)=\begin{cases} 1, \sigma^0(t) & \leq \sigma^0_{\mathrm{wm}} - 3\mathrm{dB} \\ 0, \sigma^0(t) & > \sigma^0_{\mathrm{wm}} - 3\mathrm{dB} \end{cases} \tag{3}$$

where σ^0_{wm} is the winter (June to August) mean σ°. This thresholding method has been successfully applied in the melt detection on the Larsen C Ice Shelf (Luckman et al. 2014). The actual scatterometer measurements are always noisy (Long, Hardin, and Whiting 1993). The great fluctuations of σ° in dry snow packs may lead to the misidentifications of melt signals. C band backscatter in dry snow zone is generally weak and lower than – 14 dB due to the deep penetration (Arigony-Neto et al. 2009). For a melting pixel, two conditions therefore should be satisfied in advance. Firstly, σ^0_{wm} should be greater than – 14 dB. Secondly, the minimum of winter σ° should be 3 dB greater than the minimum of summer (December to February) σ°.

3.2. Melt pond detection

Melt ponds on the SIS were mapped to assist in the interpretation of local discrepancies of snowmelt detected by AMSR2 and ASCAT. A modified normalized difference water index adapted for ice ($\mathrm{NDWI_{ice}}$) proposed by Yang and Smith (2013) was used in melt pond extraction based on Landsat 8 image:

$$\mathrm{NDWI_{ice}} = (\mathrm{B} - \mathrm{R})/(\mathrm{B} + \mathrm{R}) \tag{4}$$

where B and R represent the blue and red bands respectively. Compared with the classical NDWI index (i.e. the normalized ratio between green and near infrared bands), $\mathrm{NDWI_{ice}}$ can enhance the spectral contrast between the dry snow/ice surfaces and water bodies. Regions with slush/water will result in pixels with higher $\mathrm{NDWI_{ice}}$ values. A threshold of 0.12 was used to distinguish water bodies over SIS according to Bell et al. (2017).

4. Comparison of snowmelt

Daily snowmelt on the SIS was determined by AMSR T_b and ASCAT σ° time series (Figure 2(a)). The SIS began to melt in December. After reaching the peak in the next January, the melt area shrank quickly in February. The SIS became almost totally frozen in late February. Daily melt area detected by AMSR2 and ASCAT was very close but show great differences in the early and late melt season. Melt season can last for more than 3 months on the SIS (Figure 2(b)).

Cumulative melt area (i.e. the sum of daily melt area) detected by AMSR2 and ASCAT was 2.24×10^6 km^2 and 2.01×10^6 km^2 respectively during 2014–2015. Melt area mapped by the two sensors suggest that almost the whole SIS melted. Significant local discrepancies were found along the grounding line. AMSR2 recognized much more extensive melt area, snowmelt was found to expand towards the inland for

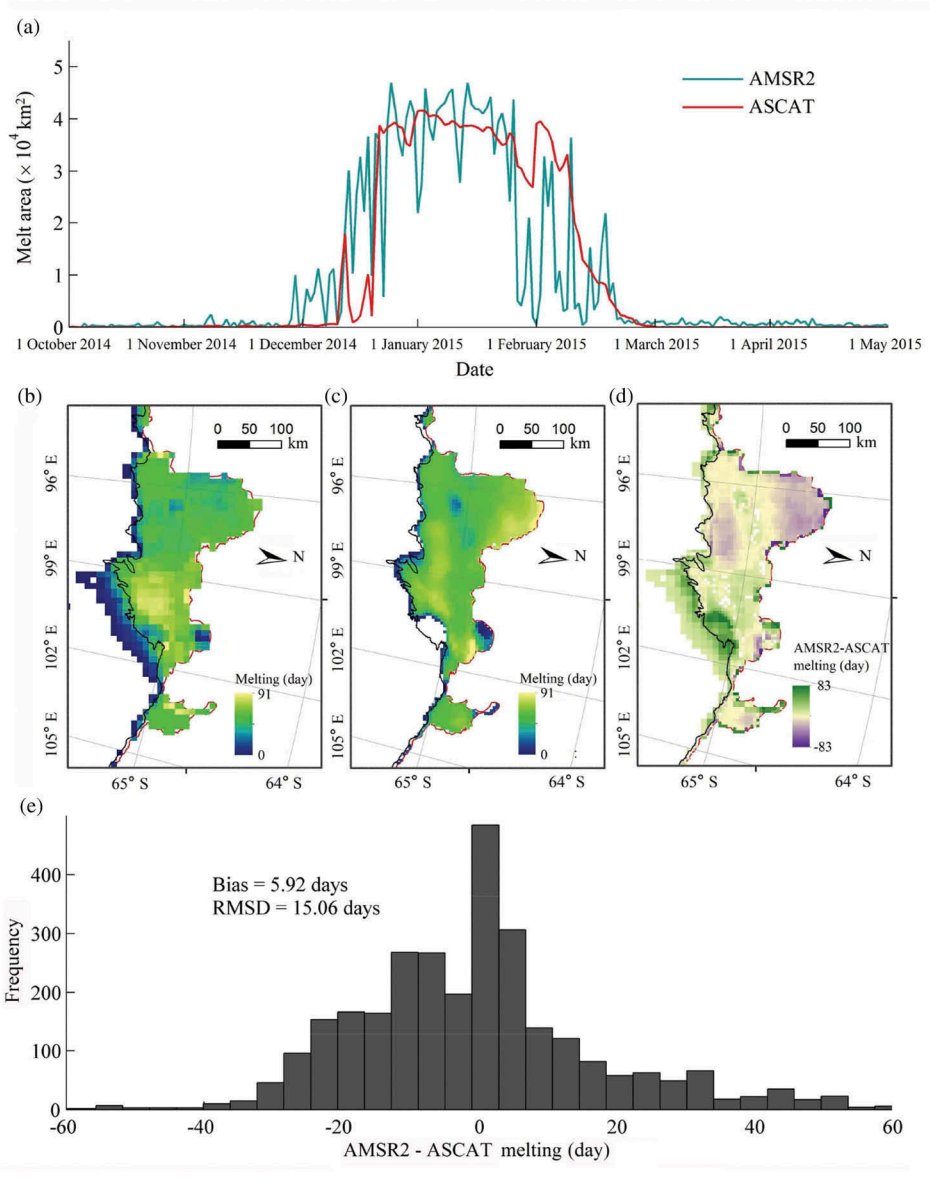

Figure 2. Snowmelt detected by AMSR2 and ASCAT during 2014–2015. (a) Daily melt area. (b) AMSR2 melting days. (c) ASCAT melting days. (d) Spatial distribution of the difference between AMSR2 and ASCAT melting days. (e) Frequency of the difference between AMSR2 and ASCAT melting days.

kilometres. The inner border of melt area mapped by ASCAT agreed well with the grounding line except for the places where blue ice and rock outcrops located.

Melting days derived by AMSR2 and ASCAT agreed well in the most part of the eastern SIS, however, showed great local discrepancies in the west part where ASCAT derived melting days were significant more than that derived by AMSR2 (Figure 2(b–d)). However, in the blue ice and rocky area, AMSR2 derived melting days were more than

20 days, while no snowmelt was recognized by ASCAT. The bias and root mean square deviation (RMSD) between the melting days derived by AMSR2 and ASCAT are 5.9 days and 15.1 days respectively (Figure 2(e)).

5. Discussion

The Antarctic ice sheet surface is generally flat and homogeneous, but also shows heterogeneities for a very limited area where snow dunes, blue ice and rock outcrops are located. A large area of blue ice in the grounding zone of the SIS can be clearly seen in the Landsat Image Mosaic of Antarctica (LIMA) image (Figure 3(a)). Moreover, rock outcrops obtained from the Antarctic digital database (ADD) are found to distribute near the blue ice (Fox, Paul, and Cooper 1994). Several small islands beneath the SIS result in the rise of the ice surface (Figure 3(b)). Large surface slopes are found in the grounding zone of the SIS. We compared melting days and slope along profile AC and DH (Figure 4). The corresponding satellite observations for point A – H are shown in Figure 5.

Melting days showed considerable variations along both profile AC and DH (Figure 4). Both the two sensors did not detect snowmelt in the first 50 km of profile AC (point A). Significant surface slope variations near the grounding line (50 km – 70 km) were accompanied by a sharp rise of melting days derived by both AMSR2 and ASCAT. Masson Island is about 300 m higher than the adjacent snow surface, leading to the significant shorter melt seasons. Generally, ASCAT recognized more melt signals than AMSR2 (point C). The large

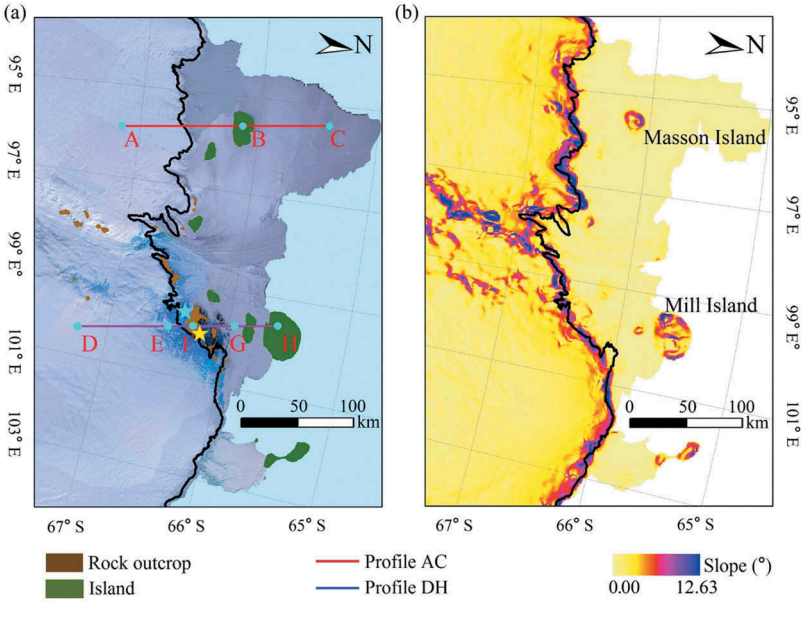

Figure 3. Surface features over the SIS. (a) Rock outcrops (brown areas) and islands (green areas) obtained from the Antarctic digital database (ADD) and NSIDC. Red lines represent profiles shown in Figure 4, A – H denote the locations of the points presented in Figures 4 and 5. Cyan and yellow stars show the positions of the melt ponds in the regions with blue ice and rocks outcrops showed in Figure 4 (c) – (f). (b) Map of slope generated by the Bamber Digital Elevation Model (DEM) was obtained from NSIDC (Bamber, Gomez-Dans, and Griggs 2009).

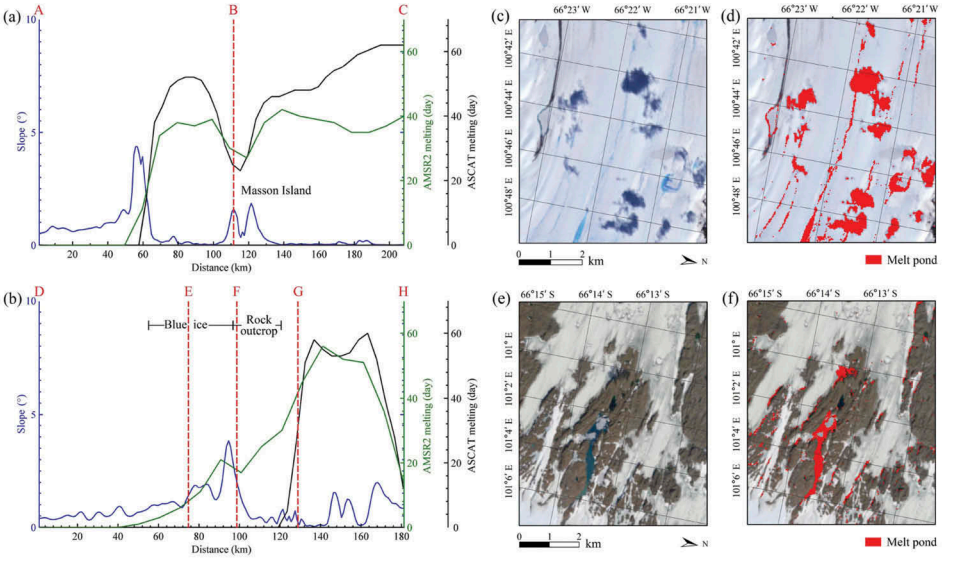

Figure 4. Surface slope (blue line), melting days derived from AMSR2 (green line) and ASCAT (black line) along profile AC (a) and DH (b). (c) and (e) are the Landsat images that illustrate the melt ponds in the regions with blue ice and rock outcrops respectively. (d) and (f) are the corresponding melt ponds extraction. The Landsat 8 image was acquired on 13 January 2015 and obtained from the United States Geological Survey (Roy et al. 2014).

penetration depth at C band making the ASCAT measurements sensitive to the remaining subsurface liquid water after the refreezing of the surface in summer (Ashcraft and Long 2006). A recent study found that ASCAT can detect liquid water at depths of up to 0.75 m (Bevan et al. 2018), while Ka band penetration depth in coarse grain snowpack (e.g. the percolation zone) is less than 0.05 m (Guerreiro et al. 2016) and is even shallow when the snowpack is melting. This also explains more extensive ASCAT derived melt area in late melt season (Figure 2(a)). ASCAT derived melting days was less than that detected by AMSR2 in the regions with surface fluctuations, such as the grounding zone and the Masson Island (point B). Surface slope complicates the backscatter received by ASCAT in the Antarctic (Fraser, Young, and Adams 2014; Fraser et al. 2016), and makes it challenging to detect snowmelt.

The underlying surface is more complex along profile DH (Figure 4(b)). AMSR2 detected snowmelt since 40 km, however, no melt signals were recognized by ASCAT until 120 km. A wide range of blue ice (point E) and rock outcrops (point F) are distributed between these two points. Melt ponds always occur in the regions with rock outcrop and blue ice due to the relatively lower surface albedo and enhanced absorption of solar radiation compared with the snow surface (Zhou et al. 2019; Lenaerts et al. 2016). This phenomenon was also found on SIS based on the Landsat 8 image obtained on 13 January 2015 (Figure 4(c–f)). It is a significant limitation that ASCAT may fail to recognize melt signals in blue ice areas because specular reflection dominates the backscatter (Zhou et al. 2019). Rock outcrops are characterized by very stable backscatter in C band (Parajka et al. 2005). ASCAT backscatter from blue ice and rocky surface both showed little change during melt season and failed to detect snowmelt (Figure 5).

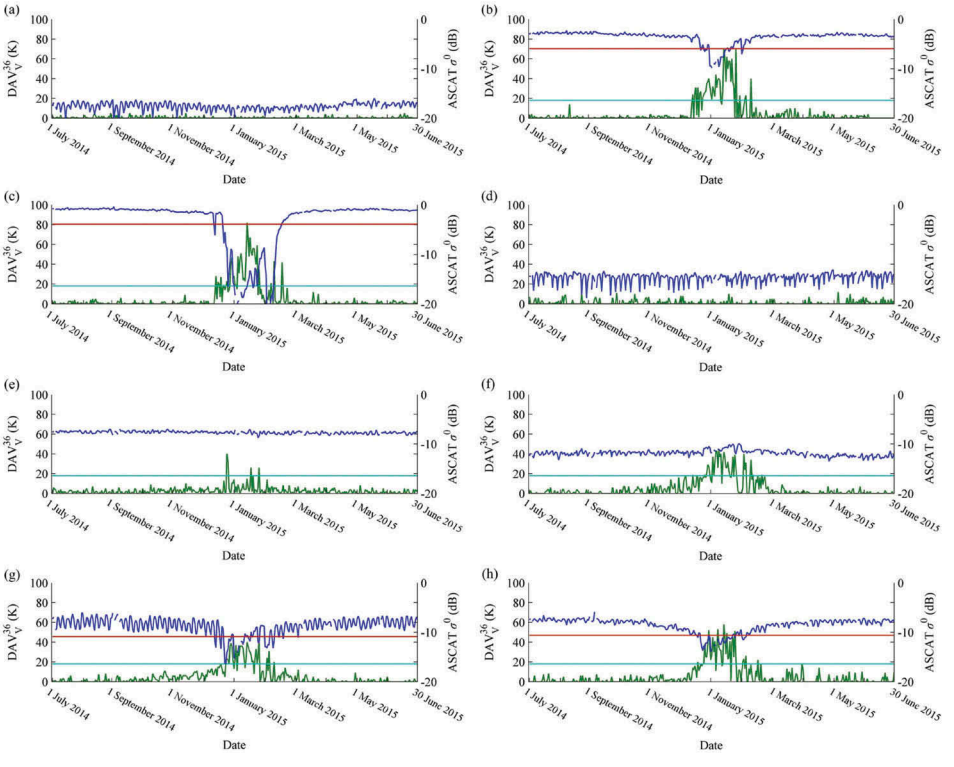

Figure 5. AMSR2 DAV$_V^{36}$ (green lines) and ASCAT σ° (blue lines) during 2014–2015. (a) – (f) show the comparisons for point A – H. The cyan and red lines represent the thresholds used for AMSR2 and ASCAT snowmelt detection.

It is also difficult for radiometer to detect surface snowmelt in bare ice area (Mote and Anderson 1995). Nevertheless, melt signals were still recognized by AMSR2 in the regions with plenty of blue ice and rock outcrops (point E and F in Figure 5), possibly due to the relatively coarse spatial resolution and shallower snowpack penetration which allow the detection of snowmelt in subpixel.

As illustrated above, AMSR2 and ASCAT show different performances in snowmelt detection in the regions with complex terrain, blue ice and rock outcrops due to the differences in operating frequencies and imaging modes. Satellite acquisition time could be another important reason for the differences in freeze/thaw retrievals because melting and refreezing can occur at any time of the day (Zheng et al. 2018). Picard and Fily (2006) found the diurnal Antarctic melt area variations are consistently near sinusoidal. On average, AMSR2 observed the SIS on 14:49 ± 17 minutes (a warm period) and 23:33 ± 17 minutes (a cold period) in ascending and descending passes respectively, which can make full use of the DAV$_V^{36}$ algorithm (Zheng et al. 2018). By contrast, the ASCAT product achieves enhanced resolution by sacrificing temporal resolution. At present, we are not able to validate the melt detection methods for two reasons: (1) no reliable and continuous snow wetness measurements on the SIS are available, and (2) significant differences can exist between in situ measurements and satellite estimations due to the different spatial scales (i.e. representativeness errors) (Lyu et al. 2017).

6. Conclusions

This study compares the snowmelt detected by the passive and active microwave sensors. The SIS began to melt in December. After reaching the peak in the next January, melt area shrank quickly in February. The SIS became almost totally frozen in late February. Melt area detected by AMSR2 and ASCAT was consistent on most of the SIS, however, also showed significant local discrepancies. Snowmelt detected by the two sensors differs in the regions with complex terrain, blue ice and rock outcrops. There exist complementary natures of radiometer and scatterometer in snowmelt detection. With the increase of microwave sensors, further work will focus on the combination of different microwave sensors to provide a better view of the surface snowmelt on the ice sheets. An automatic snowmelt detection method based on multisource satellite data is already in progress.

Acknowledgements

The authors would like to thank the Japan Aerospace Exploration Agency and Brigham Young University for providing the AMSR2 and ASCAT data respectively. We are grateful to the editor and anonymous reviewers for their insightful comments

Disclosure statement

No potential conflict of interest was reported by the authors.

Funding

This research is funded by the National Natural Science Foundation of China (NSFC) (41531069, 41776200, 41376187).

References

Apgar, J. D., J. M. Ramage, A. M. Rose, and M. Patrick. 2007. "AMSR–E Algorithm for Snowmelt Onset Detection in Sub-Arctic Heterogeneous Terrain." *Hydrological Processes* 21: 1587–1596.

Arigony-Neto, J., H. Saurer, J. C. Simões, F. Rau, R. Jaña, S. Vogt, and H. Gossmann. 2009. "Spatial and Temporal Changes in Dry-Snow Line Altitude on the Antarctic Peninsula." *Climatic Change* 94 (1–2): 19–33. doi:10.1007/s10584-009-9550-1.

Ashcraft, I. S., and D. G. Long. 2006. "Comparison of Methods for Melt Detection over Greenland Using Active and Passive Microwave Measurements." *International Journal of Remote Sensing* 27 (12): 2469–2488. doi:10.1080/01431160500534465.

Bamber, J. L., J. L. Gomez-Dans, and J. A. Griggs. 2009. "A New 1 Km Digital Elevation Model of the Antarctic Derived from Combined Satellite Radar and Laser Data – Part 1: Data and Methods." *The Cryosphere* 3 (1): 101–111.

Bell, R. E., W. Chu, J. Kingslake, I. Das, M. Tedesco, K. J. Tinto, C. J. Zappa, M. Frezzotti, A. Boghosian, and W. S. Lee. 2017. "Antarctic Ice Shelf Potentially Stabilized by Export of Meltwater in Surface River." *Nature* 544 (7650): 344–348. doi:10.1038/nature22048.

Bevan, S. L., A. J. Luckman, P. Kuipers Munneke, B. Hubbard, B. Kulessa, and D. W. Ashmore. 2018. "Decline in Surface Melt Duration on Larsen C Ice Shelf Revealed by the Advanced Scatterometer (ASCAT)." *Earth and Space Science* 5 (10): 578–591. doi:10.1029/2018EA000421.

Figa-Saldaña, J., J. J. W. Wilson, E. Attema, R. Gelsthorpe, M. R. Drinkwater, and A. Stoffelen. 2002. "The Advanced Scatterometer (ASCAT) on the Meteorological Operational (metop) Platform:

A Follow on for European Wind Scatterometers." *Canadian Journal of Remote Sensing* 28 (3): 404–412. doi:10.5589/m02-035.

Fox, A. J., A. Paul, and R. Cooper. 1994. "Measured Properties of the Antarctic Ice Sheet Derived from the SCAR Antarctic Digital Database." *Polar Record* 30 (174): 201–206. doi:10.1017/S0032247400024268.

Fraser, A. D., M. A. Nigro, S. R. M. Ligtenberg, B. Legresy, M. Inoue, J. J. Cassano, P. Kuipers Munneke, et al. 2016. "Drivers of ASCAT C Band Backscatter Variability in the Dry Snow Zone of Antarctica." *Journal of Glaciology* 62 (231): 170–184. doi:10.1017/jog.2016.29.

Fraser, A. D., N. W. Young, and N. Adams. 2014. "Comparison of Microwave Backscatter Anisotropy Parameterizations of the Antarctic Ice Sheet Using ASCAT." *IEEE Transactions on Geoscience and Remote Sensing* 52 (3): 1583–1595. doi:10.1109/TGRS.2013.2252621.

Guerreiro, K., S. Fleury, E. Zakharova, F. Rémy, and A. Kouraev. 2016. "Potential for Estimation of Snow Depth on Arctic Sea Ice from CryoSat-2 and SARAL/AltiKa Missions." *Remote Sensing of Environment* 186: 339–349. doi:10.1016/j.rse.2016.07.013.

Hallikainen, M. T., F. Ulaby, and M. Abdelrazik. 1986. "Dielectric Properties of Snow in the 3 to 37 GHz Range." *IEEE Transactions On Antennas & Propagation* 34 (11): 1329–1340.

Hihara, T., M. Kubota, and A. Okuro. 2015. "Evaluation of Sea Surface Temperature and Wind Speed Observed by GCOM-W1/AMSR2 Using in Situ Data and Global Products." *Remote Sensing of Environment* 164: 170–178.

Imaoka, K., M. Kachi, H. Fujii, H. Murakami, M. Hori, A. Ono, T. Igarashi, et al. 2010. "Global Change Observation Mission (GCOM) for Monitoring Carbon, Water Cycles, and Climate Change." *Proceedings of the IEEE* 98 (5): 717–734. doi:10.1109/JPROC.2009.2036869.

Kuipers Munneke, P., A. J. Luckman, S. L. Bevan, C. J. P. P. Smeets, E. Gilbert, M. R. van Den Broeke, W. Wang, et al. 2018. "Intense Winter Surface Melt on an Antarctic Ice Shelf." *Geophysical Research Letters* 45 (15): 7615–7623. doi:10.1029/2018GL077899.

Lenaerts, J. T. M., S. Lhermitte, R. Drews, S. R. M. Ligtenberg, S. Berger, V. Helm, C. J. P. P. Smeets, et al. 2016. "Meltwater Produced by Wind–Albedo Interaction Stored in an East Antarctic Ice Shelf." *Nature Climate Change* 7 (1): 58–62. doi:10.1038/nclimate3180.

Lindsley, R. D., and D. G. Long 2010. "Adapting the SIR Algorithm to ASCAT." *International Geoscience and Remote Sensing Symposium (IGARSS)*. IEEE, 3402–3405. doi:10.1109/IGARSS.2010.5650207.

Liu, H., L. Wang, and K. C. Jezek. 2005. "Wavelet-transform Based Edge Detection Approach to Derivation of Snowmelt Onset, End and Duration from Satellite Passive Microwave Measurements." *International Journal of Remote Sensing* 26 (21): 4639–4660. doi:10.1080/01431160500213342.

Liu, H., L. Wang, and K. C. Jezek. 2006. "Automated Delineation of Dry and Melt Snow Zones in Antarctica Using Active and Passive Microwave Observations from Space." *IEEE Transactions on Geoscience & Remote Sensing* 44 (8): 2152–2163.

Long, D. G., P. J. Hardin, and P. T. Whiting. 1993. "Resolution Enhancement of Spaceborne Scatterometer Data." *IEEE Transactions on Geoscience and Remote Sensing* 31 (3): 700–715. doi:10.1109/36.225536.

Luckman, A., A. Elvidge, D. Jansen, B. Kulessa, P. Kuipers Munneke, J. King, and N. E. Barrand. 2014. "Surface Melt and Ponding on Larsen C Ice Shelf and the Impact of Föhn Winds." *Antarctic Science* 26 (6): 625–635. doi:10.1017/S0954102014000339.

Lyu, H., K. A. Mccoll, X. Li, C. Derksen, A. Berg, T. A. Black, E. Euskirchen, et al. 2017. "Validation of the SMAP Freeze/Thaw Product Using Categorical Triple Collocation." *Remote Sensing of Environment* 205 :329–337. doi:10.1016/j.rse.2017.12.007.

McCabe, M. F., P. Chylek, and M. K. Dubey. 2011. "Detecting Ice-Sheet Melt Area over Western Greenland Using MODIS and AMSR-E Data for the Summer Periods of 2002-2006." *Remote Sensing Letters* 2 (2): 117–126. doi:10.1080/01431161.2010.501830.

Monahan, P. A., and J. Ramage. 2010. "AMSR-E Melt Patterns on the Southern Patagonia Icefield." *Journal of Glaciology* 56 (198): 699–708. doi:10.3189/002214310793146197.

Mote, T. L., and M. R. Anderson. 1995. "Variations in Snowpack Melt on the Greenland Ice Sheet Based on Passive-Microwave Measurements." *Journal of Glaciology* 41 (137): 51–60.

Parajka, J., K. Scipal, R. Merz, G. Blöschl, W. Wagner, R. Kidd, Z. Bartalis, and V. Naeimi 2005. *Spatial and Temporal Dynamics of Soil Moisture in Ungauged* Basins. *Interim Report, Hydrology of Austria Programme (HÖ), Austrian Academy of Sciences*. https://publik.tuwien.ac.at/files/pub-geo_1285.pdf.

Picard, G., and M. Fily. 2006. "Surface Melting Observations in Antarctica by Microwave Radiometers: Correcting 26-year Time Series from Changes in Acquisition Hours." *Remote Sensing of Environment* 104 (3): 325–336. doi:10.1016/j.rse.2006.05.010.

Roy, D. P., M. A. Wulder, T. R. Loveland, C. E. Woodcock, R. G. Allen, M. C. Anderson, D. Helder, et al. 2014. "Landsat-8: Science and Product Vision for Terrestrial Global Change Research." *Remote Sensing of Environment* 145 :154–172. doi:10.1016/j.rse.2014.02.001.

Scambos, T., C. Hulbe, M. Fahnestock, and J. Bohlander. 2000. "The Link between Climate Warning and Break-up of Ice Shelves in the Antarctic Peninsula." *Journal of Glaciology* 46 (154): 516–530. doi:10.3189/172756500781833043.

Scambos, T. A., T. M. Haran, M. A. Fahnestock, T. H. Painter, and J. Bohlander. 2007. "MODIS-Based Mosaic of Antarctica (MOA) Data Sets: Continent-Wide Surface Morphology and Snow Grain Size." *Remote Sensing of Environment* 111: 242–257. doi:10.1016/j.rse.2006.12.020.

Semmens, K. A., J. Ramage, A. Bartsch, and G. E. Liston. 2013. "Early Snowmelt Events: Detection, Distribution, and Significance in a Major Sub-Arctic Watershed." *Environmental Research Letters* 8: 014020. doi:10.1088/1748-9326/8/1/014020.

Steiner, N., and M. Tedesco. 2014. "A Wavelet Melt Detection Algorithm Applied to Enhanced-Resolution Scatterometer Data over Antarctica (2000-2009)." *The Cryosphere* 8: 25–40. doi:10.5194/tc-8-25-2014.

Tedesco, M. 2007. "Snowmelt Detection over the Greenland Ice Sheet from SSM/I Brightness Temperature Daily Variations." *Geophysical Research Letters* 34: L02504. doi:10.1029/2006GL028466.

Tedesco, M., W. Abdalati, and H. J. Zwally. 2007. "Persistent Surface Snowmelt over Antarctica (1987–2006) from 19.35 GHz Brightness Temperatures." *Geophysical Research Letters* 34: L18504. doi:10.1029/2007gl031199.

Torres, R., P. Snoeij, D. Geudtner, D. Bibby, M. Davidson, E. Attema, P. Potin, et al. 2012. "GMES Sentinel-1 Mission." *Remote Sensing of Environment* 120 :9–24. doi:10.1016/j.rse.2011.05.028.

Urbini, S., L. Cafarella, A. Zirizzotti, I. E. Tabacco, C. Bottari, J. A. Baskaradas, and N. Young. 2010. "Radio Echo Sounding Data Analysis of the Shackleton Ice Shelf." *Annals of Geophysics* 53 (2): 79–87. doi:10.4401/ag-4563.

Yang, K., and L. C. Smith. 2013. "Supraglacial Streams on the Greenland Ice Sheet Delineated from Combined Spectral-Shape Information in High-Resolution Satellite Imagery." *IEEE Geoscience and Remote Sensing Letters* 10 (4): 801–805. doi:10.1109/LGRS.2012.2224316.

Zheng, L., C. Zhou, and Q. Liang. 2019. "Variations in Antarctic Peninsula Snow Liquid Water during 1999–2017 Revealed by Merging Radiometer, Scatterometer and Model Estimations." *Remote Sensing of Environment* 232: 111219. doi:10.1016/j.rse.2019.111219.

Zheng, L., C. Zhou, R. Liu, and Q. Sun. 2018. "Antarctic Snowmelt Detected by Diurnal Variations of AMSR-E Brightness Temperature." *Remote Sensing* 10 (9): 1391. doi:10.3390/rs10091391.

Zhou, C., L. Zheng, Q. Sun, and R. Liu. 2019. "Amery Ice Shelf Surface Snowmelt Detected by ASCAT and Sentinel-1." *Remote Sensing Letters* 10 (5): 430–438. doi:10.1080/2150704X.2018.1553317.

Zwally, H. J., M. A. Beckley, A. C. Brenner, and M. B. Giovinetto. 2002. "Motion of Major Ice-Shelf Fronts in Antarctica from Slant-Range Analysis of Radar Altimeter Data, 1978-98." *Annals of Glaciology* 34 (1): 255–262. doi:10.3189/172756402781817653.